

# Resonant subgap current transport in Josephson field effect transistor

E. V. Bezuglyi,<sup>1,2</sup> E. N. Bratus',<sup>1</sup> and V. S. Shumeiko<sup>2</sup>

<sup>1</sup>*B.Verkin Institute for Low Temperature Physics and Engineering, Kharkiv 61103, Ukraine*

<sup>2</sup>*Chalmers University of Technology, S-41296 Göteborg, Sweden*

We study theoretically the current-voltage characteristics (IVCs) of the Josephson field effect transistor - a ballistic SNINS junction with superconducting (S) electrodes confining a planar normal metal region (N), which is controlled by the gate induced potential barrier (I). The calculations were performed using the computation technique developed earlier for long single-channel junctions in the coherent multiple Andreev reflections (MAR) regime. We find significant difference of the subgap current structure in these junctions compared to the subharmonic gap structure in tunnel junctions and atomic-size point contacts. For long junctions, whose length significantly exceeds the coherence length, the IVC exhibits current peaks at multiples (harmonics) of the difference  $\delta_m$  between the static Andreev levels,  $eV_n = n\delta_m$ . Moreover, the averaged IVC follows the power rather than exponential behavior, and has a universal scaling with the junction transparency. This result is qualitatively understood using an analytical approach based on the concept of resonant MAR trajectories. In shorter junctions whose length is comparable to the coherence length, the IVC has an exponential form common for point contacts, however the current structures appear at the subharmonics of the Andreev interlevel distance,  $eV_n = \delta_m/n$  rather than the gap subharmonics  $2\Delta/n$ .

## I. INTRODUCTION

In a number of experiments, the current-voltage characteristics (IVCs) were measured in superconductor-normal metal-superconductor (SNS) junctions consisting of high-mobility two-dimensional electron gas (2DEG) connected to two bulk superconducting electrodes.<sup>1-6</sup> In these devices, the electrodes have a large width  $W$  up to  $40 \mu\text{m}$ , while the distance  $L$  between the electrodes varies between  $0.2 - 1 \mu\text{m}$ . This is comparable or larger than the normal coherence length  $\xi_N = \hbar v_F / \Delta$ , where  $v_F$  is the Fermi velocity in the 2DEG, but much smaller than the elastic and inelastic scattering lengths. The interface resistance is rather small and corresponds to a large transmission coefficient  $\sim 0.8$ .<sup>4,6</sup> These junctions show well pronounced Josephson effect.

Most of these 2DEG structures were fabricated in effort to develop a Josephson field effect transistor (JOFET).<sup>7</sup> In this device, schematically shown in Fig. 1(a) (see, e.g., Ref. 5), the Josephson current is controlled by the gate voltage which changes the carrier concentration within the area just beneath the gate and thus creates a potential barrier across the 2DEG layer. Assuming the width of this barrier much smaller than  $L$ ,

one can consider such device as a practical realization of the theoretical model of a wide SNINS junction with tunable potential barrier inside the 2D normal metal layer, Fig. 1(b). The dc and ac Josephson currents in such junctions were studied in Refs. 8-10. In our paper, we examine the dissipative charge transport through JOFET in the regime of given applied voltage and predict a markedly different subgap current structure compared to tunnel junctions and point contacts, originating from quantized Andreev bound states in the normal layer.

Assuming the dephasing length much larger than the junction length, we consider coherent multiple Andreev reflection (MAR) regime, the theory of which has been mostly developed for single-channel contacts: short junctions with the length  $L \ll \xi_N$ <sup>11-13</sup> and long junctions with a strong scatterer.<sup>14</sup> In the multichannel transport regime, the current can be evaluated by integrating the single-channel currents over the known distribution of the normal junction transmission eigenvalues. The overall shape of IVC depends on the transmission distribution. The qualitative result for the dc current in short contacts is exponential decay at small voltage,  $I \sim D^{(2\Delta/eV)}$  for various tunnel structures,<sup>11-13,15,16</sup> while for diffusive constrictions<sup>17</sup>  $I \sim V^{1/2}$ . Furthermore, the IVCs contain current structures at gap subharmonics,  $eV = 2\Delta/n$  (subharmonic gap structure).

In long multichannel junctions, the integration over channels, which is equivalent to averaging over effective lengths of the channels, would average out, as one could expect, the current resonances found in the single channel.<sup>14</sup> However, as we will show in this paper, the resonances survive, due to the length cut-off of the conducting channels, while the averaging results in a universal scaling behavior in the limit of long junctions, and the power law dependence of the overall IVCs at small voltage.

The structure of the paper is the following. After brief discussion of the MAR theory for a single channel and its generalization to the multichannel case in Section II, we present the results of numerical calculation of the IVC of a multichannel junction in Section III. This calculation indicates the existence of two qualitatively different regimes. In a relatively

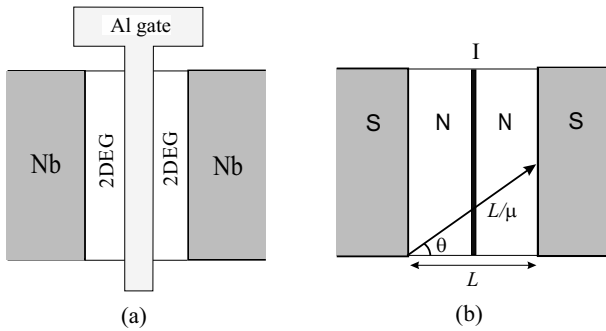


FIG. 1. Experimental JOFET setup<sup>5</sup> (a) and the theoretical model (b) of the gated SNS junction. The role of a controlled tunnel barrier (I) is played by the gate potential. The inclined line depicts the electron trajectory with the length  $L/\mu$ ,  $\mu = \cos \theta$ .

short junctions with only two Andreev levels for the majority of quasiparticles, the IVC has an exponential form and exhibits features at subharmonics of the maximum value  $\delta_m$  of the interlevel distance. In the limit of a long junction (multi-level situation), the IVC is power-like, and the resonant features occur at the voltages which are multiples (harmonics) of  $\delta_m$ . In order to explain the physics of these results, we develop in Section IV an analytical approach to the calculation of the IVC for long multi-mode junctions. We show that the single- and two-particle currents scale as  $R_N^{-1}$ , where  $R_N \sim D^{-1}$  is the normal resistance of the junction, and the  $n$ -particle currents ( $n > 2$ ) are described by *universal* dependencies  $I_n = (\Delta\sqrt{D}/eR_N)F_n(eV/\Delta)$ , thus scaling as  $D^{3/2}$ .

## II. CALCULATION SCHEME

In this Section, we briefly discuss our calculation method based on the results of calculation of the dc current for the single-mode (one-dimensional, 1D) structure.<sup>14</sup> In the 1D case, the net current  $I^{1D}(V)$  is expressed through the sum of the contributions of partial  $n$ -particle spectral currents  $j_n(E)$ ,

$$I^{1D} = -\frac{e}{h} \sum_{n=1}^{\infty} n \left[ \Theta(neV - 2\Delta) \int_{\Delta-neV}^{-\Delta} dE j_n(E) \tanh \frac{E}{2T} + \int_{-\infty}^{-\Delta-neV} dE j_n(E) \left( \tanh \frac{E}{2T} - \tanh \frac{E_n}{2T} \right) \right], \quad (1)$$

where  $\Theta(x)$  is the Heaviside step function and

$$j_n(E) = \frac{8\xi\xi_n}{\Delta^2|Z(E)|^2} (e^\gamma + |r_{0-}|^2 e^{-\gamma}) (e^{\gamma_n} + |r_{n+}|^2 e^{-\gamma_n}), \quad (2)$$

$$Z(E) = \begin{pmatrix} 1, & -r_{0-} \end{pmatrix} (\hat{U}_n \hat{M}_{n0} \hat{U}_0)^{-1} \begin{pmatrix} 1 \\ r_{n+} \end{pmatrix}.$$

Here the index  $n$  indicates the shift of the energy,  $E_n = E + neV$ ,  $\exp(\gamma) = (E + \xi)/\Delta$ , and  $\xi(E) = \sqrt{(E + i0)^2 - \Delta^2}$  is the analytical function of complex energy defined in the upper half-space. The amplitudes  $r_{n\pm}$  refer to the limiting values of the following ratios of matrix elements of the  $2 \times 2$  matrix  $\hat{M}_{nm}$ :

$$r_{n+} = -\lim_{m \rightarrow +\infty} \frac{(\hat{M}_{nm})_{11}}{(\hat{M}_{nm})_{12}}, \quad r_{0-} = \lim_{m \rightarrow -\infty} \frac{(\hat{M}_{0m})_{12}}{(\hat{M}_{0m})_{22}}. \quad (3)$$

In practical calculations, the limits in Eq. (3) are truncated according to the rule: the energies  $E_m$  and  $E_n$  defined by the indices of the matrix  $\hat{M}_{nm}$  are to be located at different sides of the energy gap, with few added steps in  $m$  for better accuracy.

The matrix  $\hat{M}_{nm}$  ( $\det \hat{M} = 1$ ,  $n > m$ ) has a meaning of a transfer matrix along the MAR trajectory in the energy space across the gap,<sup>18</sup> and is defined as the product

$$\hat{M}_{nm} = \hat{T}_{n-1} \hat{U}_{n-1} \hat{T}_{n-2} \hat{U}_{n-2} \dots \hat{T}_m, \quad (4)$$

$$\hat{U}(E) = e^{-\sigma_z \gamma}, \quad \hat{T}_{2n} = (\hat{T}_{2n}^e)^{-1}, \quad \hat{T}_{2n+1} = \hat{T}_{2n+1}^h. \quad (5)$$

Here the matrices  $\hat{U}_n(E) = \hat{U}(E_n)$  describe the phase shifts of the wave functions associated with the Andreev reflection,

and  $\hat{T}_n^{e,h}$  are the real space transfer matrices of the junction in the normal state for electrons and holes, respectively. The potential barrier is modeled by a localized scatterer with the energy independent scattering amplitudes, which will be assumed identical for all conducting channels. Furthermore, we consider completely transparent NS interfaces which eliminates the Fabry-Perot interference effects, and enables us to exclude the scattering phases, thus reducing the characteristics of the scatterer to its transparency  $D$  and reflection coefficient  $R = 1 - D$ . Accordingly, the transfer matrices in Eq. (5) are composed with the transfer-matrix  $\hat{t}$  of the scatterer, and the ballistic transfer-matrices  $\hat{u}(E)$ , which describe free propagation through the normal region,

$$\hat{T}_n^{e,h}(E) = \hat{u}^{e,h}(E) \hat{t} \hat{u}^{e,h}(E), \quad \hat{t} = D^{-1/2} (1 + \sigma_x \sqrt{R}), \quad (6)$$

$$\hat{u}^{e,h}(E) = \exp \left[ i \left( p_x L \mp \sigma_z \frac{\phi}{2} \right) \right], \quad \phi(E) = \frac{L}{v_x} \left( E + \frac{eV}{2} \right).$$

In planar junction,  $v_x$  and  $p_x$  refer to the longitudinal (perpendicular to the NS boundaries) components of the particle velocity and momentum, respectively. The matrix  $\hat{T}_n$  can be written as

$$\hat{T}_n = D^{-1/2} [\exp(i\sigma_z \phi_n) - (-1)^n \sigma_x \sqrt{R}]. \quad (7)$$

One can rewrite Eqs. (5)–(7) in a more convenient form, by combining the matrices  $\hat{u}^{e,h}$  with the  $\hat{U}$ -matrices rather than  $\hat{t}$ -matrices. In such representation,

$$\hat{T}_n = D^{-1/2} [1 - (-1)^n \sigma_x \sqrt{R}], \quad \hat{U}_n = e^{-\sigma_z (\gamma_n - iE_n L/v_x)}. \quad (8)$$

Along with this transformation, we exclude the factors with unity moduli from  $Z(E)$  in Eq. (2).

Proceeding with the case of a multichannel junction, we apply the quasiclassical approach to the summation over the channels, assuming their number  $\mathcal{N}$  to be macroscopically large. Enumerating the channels by the values of their transversal momentum  $p_\perp$ , which is quantized in a multichannel 2D junction of width  $w$  as  $p_{\perp k} = \pi k \hbar / w$ ,  $k = 0, 1, \dots$ , we arrive to the following rule of the summation over the channels in the quasiclassical limit  $\mathcal{N} = p_F w / \hbar \gg 1$  ( $p_F$  is the Fermi momentum),

$$I^{2D} = \sum_{p_{\perp k} < p_F} I^{1D}(v_{x,k}) \rightarrow \frac{w}{\pi \hbar} \int_0^{p_F} dp_\perp I^{1D}(v_x) \quad (9)$$

$$= \mathcal{N} \int_0^1 d\mu q(\mu) I^{1D}(v_F \mu), \quad q(\mu) = \frac{\mu}{\sqrt{1 - \mu^2}}.$$

Here  $\mu$  is the cosine of the angle  $\theta$  of incidence of the quasiparticle at the NS boundary, see Fig. 1. For a 3D structure with the cross-section area  $S$ , where the number of channels is  $\mathcal{N} = \pi S p_F^2 / (2\pi \hbar)^2$ , we obtain

$$I^{3D} = \sum_{p_{\perp kl} < p_F} I^{1D}(v_{x,kl}) \rightarrow \frac{\pi S}{2(\pi \hbar)^2} \int_0^{p_F} p_\perp dp_\perp I^{1D}(v_x) \quad (10)$$

$$= \mathcal{N} \int_0^1 d\mu q(\mu) I^{1D}(v_F \mu), \quad q(\mu) = 2\mu.$$

The number of channels  $\mathcal{N}$  can be then excluded through the relation to the normal conductance  $R_N^{-1} = (2e^2/h)D\mathcal{N}$ , which is a sum of contributions  $(2e^2/h)D$  of separate conducting channels in the normal state.

In what follows, we assume the temperature to be much smaller than the energy gap  $2\Delta$  in the superconducting electrodes, which results in the following expression used in our calculations of the dc current,

$$I = \frac{1}{eR_N} \sum_{n \geq 2\Delta/eV} \int_0^1 d\mu q(\mu) J_n, \quad J_n = \frac{n}{D} \int_{-neV/2}^{-\Delta} dE j_n(E). \quad (11)$$

In Eq. (11) we account for the symmetry of the spectral density  $j_n(E)$  in Eq. (2) with respect to the middle of the initial interval of integration  $\Delta - neV < E < -\Delta$ .

### III. NUMERICAL RESULTS

In Fig. 2 we present the result of computation of the IVCs for three values of the transmission coefficients and lengths of the planar (2D) SNINS junction (the results for 3D junctions are similar). For short junction,  $L = 0.3\xi_N$ , the current rapidly decays with decreasing voltage, similar to the case of a short single-mode contact; in the limit  $L \rightarrow 0$ , the results for all dimensions (being normalized by  $R_N$ ) exactly coincide. On the contrary, for comparatively long junctions,  $L = 4\xi_N$  and  $L = 10\xi_N$ , the current decreases with voltage much more slowly. Another interesting observation is that in the limit

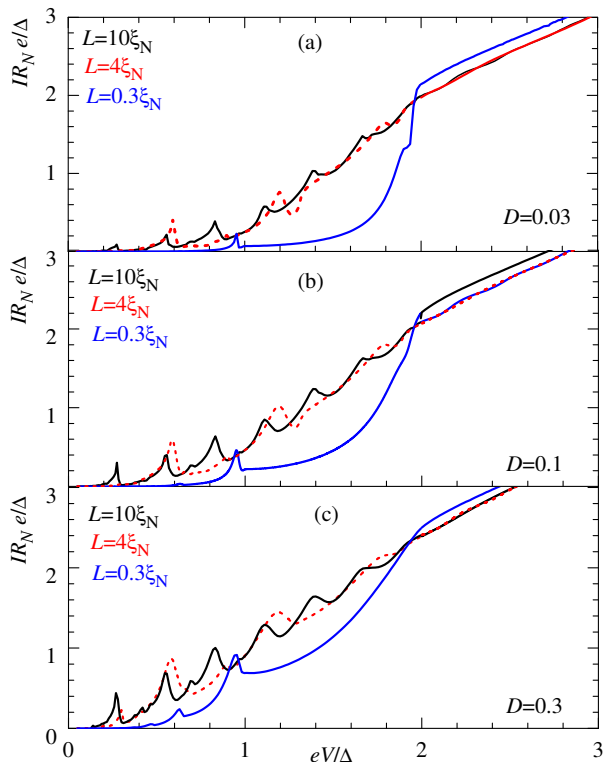


FIG. 2. (Color online) Current-voltage characteristics for different transmission coefficients  $D = 0.03$ (a),  $0.1$ (b),  $0.3$ (c) and lengths of the junction:  $L/\xi_N = 0.3$  (lower solid blue curves),  $4$  (red dashed curves), and  $10$  (upper solid black curves).

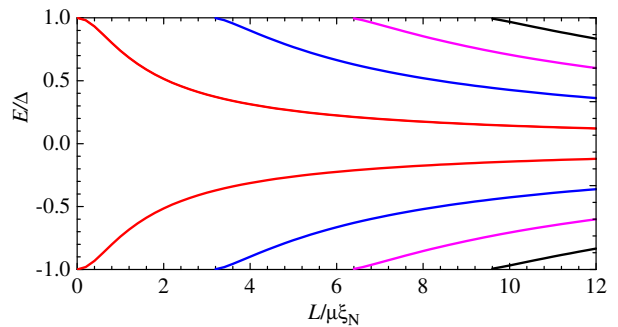


FIG. 3. Emergence and evolution of Andreev levels with the increase of the quasiparticle trajectory length.

$L \gg \xi_N$ , the smooth part of the IVC becomes independent of the junction length.

The most of characteristic features of the IVCs in the junction of finite length and width can be explained by the existence of discrete Andreev levels in equilibrium junction, and corresponding singularities in the density of the quasiparticle states. It is instructive to qualitatively examine highly resistive junctions, where this connection is the most prominent. In such junctions, the Andreev level spectrum can be approximated with the de Gennes-Saint-James bound levels<sup>19</sup> in each half of the normal layer with the length  $L/2$  (the level splitting due to the finite barrier transparency will be discussed later). Dispersion equation for these levels coincides with the one for a SNS junction of equivalent length  $L$ ,

$$\frac{EL}{\Delta\mu\xi_N} = \pi n + \arccos \frac{E}{\Delta}, \quad n = 0, \pm 1, \pm 2, \dots, \quad (12)$$

where  $|E| < \Delta$ ,  $\mu = \cos \theta$ , and  $\theta$  is the angle between the particle velocity and the normal to the junction interfaces. From Eq. (12) one can obtain simple estimates for the average inter-level distance  $\delta$  and the number of Andreev levels  $n_A$ ,

$$\delta(L, \mu) \approx \frac{\Delta}{L/\pi\mu\xi_N + 1/2}, \quad (13)$$

$$n_A(L, \mu) = 2[\text{Int}(L/\pi\mu\xi_N) + 1], \quad (14)$$

[Int( $x$ ) denotes integer part of  $x$ ]. Evolution of Andreev levels with the increase of the trajectory length  $L/\mu$  is depicted in Fig. 3.

As shown in Fig. 4, the features on the IVC of a relatively short junctions correspond to the subharmonics  $eV = \delta_m/n$ ,  $n = 1, 2, \dots$ , of the maximum distance between the two Andreev levels present in the shortest electron trajectory in these junctions,  $\delta_m = \delta(L, 1) < 2\Delta$ , which is quantitatively different from the customary structure of the energy gap subharmonics. Obviously, these features are due to the resonant MAR trajectories in the energy space whose first and last Andreev reflections occur in the neighborhood of the Andreev levels where the density of states is singular. Similar effect has been found in a diffusive SNcNS structure<sup>20</sup> where the role of the potential barrier was played by the ballistic constriction (c), and the role of Andreev levels - by the edges of the proximity induced minigap with greatly enhanced density of states; appearance of the minigap subharmonics has been also predicted for a

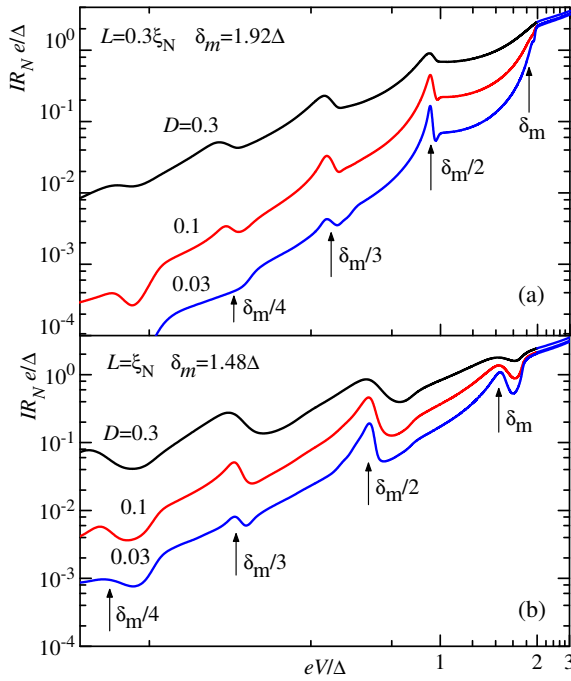


FIG. 4. (Color online) Subharmonics  $eV_n = \delta_m/n$  of the maximum interlevel distance  $\delta_m$  for the junction lengths  $L = 0.3\xi_N$  (a) and  $L = \xi_N$  (b) at different transmission coefficients.

short diffusive double-barrier junction.<sup>21</sup> Furthermore, the averaged IVC can be well approximated with the exponential dependence,  $I(V) \sim D^{(\text{const}/eV)}$ , similar to the case of  $L = 0$ , but with the constant close to  $\delta_m$  rather than to  $2\Delta$ .

A quite another picture of the IVC shape was found in longer junctions, where the number of Andreev levels is comparatively large, e.g.,  $n_A = 4$  for  $L = 4\xi_N$ , and  $n_A = 8$  for  $L = 10\xi_N$ , see Eq. (14) and Fig. 3. In this case, the IVCs plotted in Fig. 5 are non-exponential, and the resonant features correspond to multiples of the maximum interlevel distance,  $eV = n\delta_m$ ,  $n = 1, 2, \dots$ , or, in another words, to *harmonics* of  $\delta_m$ . From this we conclude that the enhanced multiparticle charge transfer is due to the MAR trajectories passing through all the Andreev resonances.

The next intriguing feature of the numerically calculated IVC for long junctions is the approximate overlap of the curves  $I(V)$  at  $eV < \Delta$  for different  $D$ , provided  $I(V)$  is normalized over  $\sqrt{D}/R_N$ , as shown in Fig. 6. Note that the smaller  $D$  is, the better this "universality" looks. This fact, as well as the universality of the averaged IVCs for large  $L$  mentioned above, motivated us to develop the analytical theory which gives a clear physical explanation of the numerically found peculiarities in the IVCs.

#### IV. ANALYTICAL RESULTS

##### A. IVC at $eV \gg \Delta$ : excess current

We start with evaluation of the excess current, i.e., voltage-independent deviation of the total current from the ohmic IVC

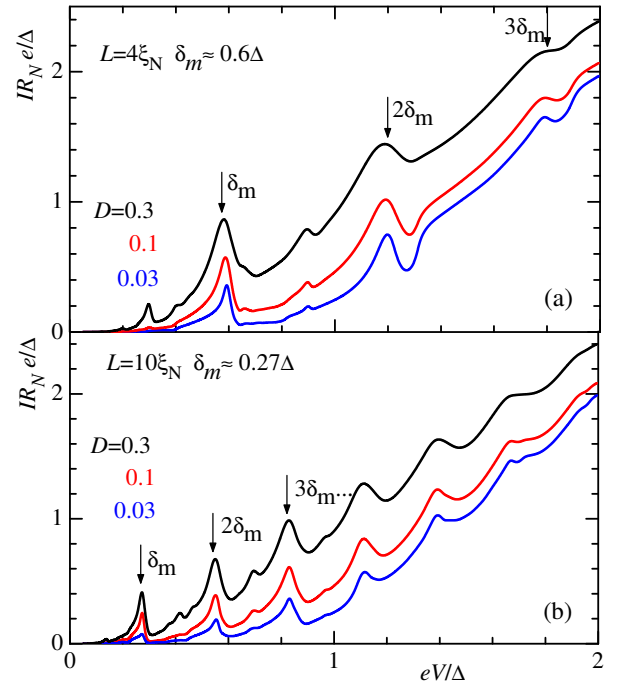


FIG. 5. (Color online) Subgap features at multiple of the maximum interlevel distance  $\delta_m$  for the junction lengths  $L = 4\xi_N$  (a) and  $L = 10\xi_N$  (b) at different transmission coefficients.

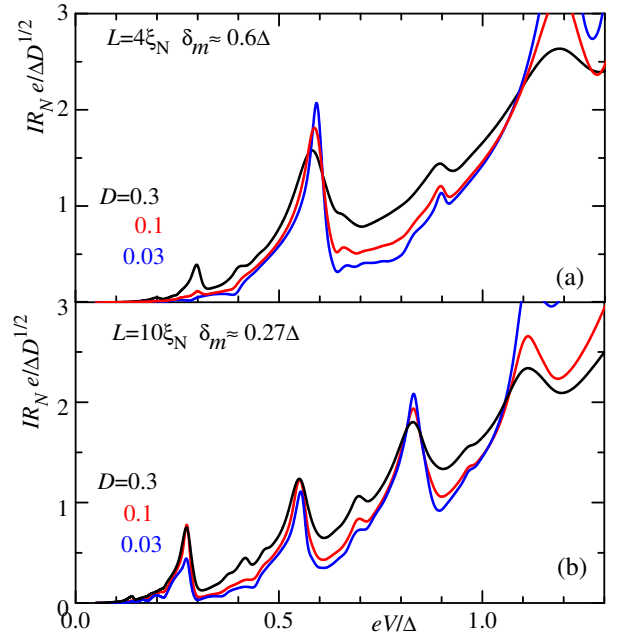


FIG. 6. (Color online) Universality of the IVCs normalized over  $\sqrt{D}/R_N$  at  $eV < \Delta$  for the junction lengths  $L = 4\xi_N$  (a) and  $L = 10\xi_N$  (b) at different transmission coefficients.

at large applied voltage  $eV \gg \Delta$ . At these voltages, the analytical result in the finite form can be obtained for all lengths and transparencies because only first two partial currents,  $J_1$  and  $J_2$ , give non-vanishing contributions to the net current, and the amplitudes  $r_{n\pm}$  approach the asymptotic values  $r_{0-} = \sqrt{R}$ ,  $r_{n+} = (-1)^n \sqrt{R}$ . Since the energy  $E_1$  is large,  $E_1 \gg \Delta$ , the

spectral current  $j_1(E)$  can be approximated as

$$j_1(E) \approx \frac{4D\xi[2E - D(E - \xi)]}{[2\xi + D(E - \xi)]^2 + 4R\Delta^2 \sin^2 \phi}, \quad (15)$$

where  $\phi = E\tilde{L}/\Delta$  and  $\tilde{L} = L/\xi_N\mu$ . In Eq. (15) we replaced  $E \rightarrow -E$  and therefore assume the integration limits  $(\Delta, eV/2)$  in Eq. (11). Within the first approximation ( $E \gg \Delta$ ,  $j_1 \approx 2D$ ), the current  $J_1$  is given by  $eV$ , which results in a normal Ohm's law for the net current  $I$ . The contribution of  $J_1$  to the excess current is related to the next term in its expansion over  $\Delta/eV$ , which is associated with the energies  $E \sim \Delta$ ,

$$J_1^{\text{exc}} = 2 \int_{\Delta}^{\infty} dE \left\{ \frac{2\xi[2E - D(E - \xi)]}{[2\xi + D(E - \xi)]^2 + 4R\Delta^2 \sin^2 \phi} - \frac{E}{\xi} \right\}. \quad (16)$$

The contribution of the second current consists of two parts: in  $J_2^{(1)}$ , the energy  $E_1$  changes inside the gap; in  $J_2^{(2)}$ ,  $E_1$  is outside the gap. Denoting  $E_1 \rightarrow -E$ , we get

$$J_2^{(1)} = 4D \int_0^{\Delta} \frac{dE}{D^2 + 4R \sin^2[\gamma(E) - \phi]},$$

$$J_2^{(2)} = 4D \int_{\Delta}^{\infty} \frac{\Delta^2 dE}{[2\xi + D(E - \xi)]^2 + 4R\Delta^2 \sin^2 \phi},$$

where  $\gamma(E) = \arccos(E/\Delta)$ . The last integral is combined with  $J_1^{\text{exc}}$ , and the general formula for the excess current reads

$$I^{\text{exc}} = \frac{2}{eR_N} \int_0^1 d\mu q(\mu) \left( 2D \int_0^{\Delta} \frac{dE}{D^2 + 4R \sin^2[\gamma(E) - \phi]} + \int_{\Delta}^{\infty} dE \left\{ \frac{2E[2\xi + D(E - \xi)]}{[2\xi + D(E - \xi)]^2 + 4R\Delta^2 \sin^2 \phi} - \frac{E}{\xi} \right\} \right) \quad (17)$$

The behavior of the excess current as a function of the junction length described by Eq. (17), is shown in Fig. 7.

In the limit of a short junction,  $L \ll \xi_N$ , Eq. (17), taken in the main approximation, reproduces known result for a single-mode junction (in terms of the normal junction resistance),

$$I^{\text{exc}} = \frac{\Delta}{eR_N} \frac{D}{R} \left[ 1 - \frac{D^2}{2\sqrt{R}(1+R)} \ln \frac{1+\sqrt{R}}{1-\sqrt{R}} \right], \quad L \ll \xi_N. \quad (18)$$

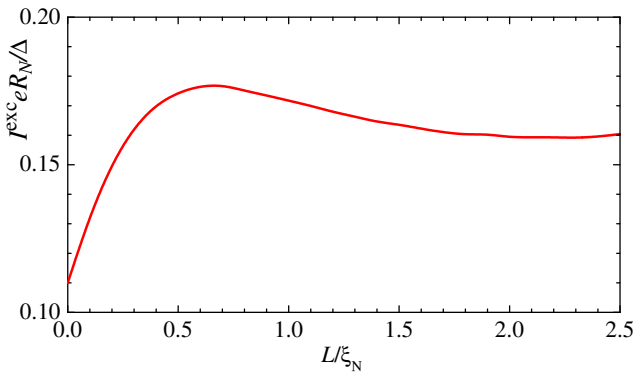


FIG. 7. Excess current vs junction length for the transparency  $D = 0.1$ . The values of  $I^{\text{exc}}$  in the limits  $L \ll \xi_N$  and  $L \gg \xi_N$  are 0.11 and 0.16, respectively [see Eqs. (18) and (24)].

In the limits  $D \ll 1$  and  $R \ll 1$ , Eq. (18) reads

$$I^{\text{exc}} = \frac{\Delta}{eR_N} \begin{cases} D, & D \ll 1; \\ 8/3, & R \ll 1. \end{cases} \quad (19)$$

In the case of a long junction,  $L \gg \xi_N$ , the integrands in Eq. (17) involve rapidly oscillating functions of  $E$  and  $\mu$ . In order to obtain an analytic result within the main approximation in  $\xi_N/L$ , we introduce the following approach which will be systematically used below. Let us consider the integral

$$A(\lambda) = \int_a^b dx f[x, \lambda z(x)], \quad \lambda \gg 1, \quad f(x, y + 2\pi) = f(x, y), \quad (20)$$

where  $f(x, y)$  and  $z(x)$  smoothly vary at the distances much larger than  $\lambda^{-1}$ . First, we introduce  $z$  as a new variable and split the whole interval of  $z$  over small elementary intervals of the length  $p = 2\pi/\lambda \ll 1$ ,

$$A(\lambda) = \sum_{k=0}^{k_{\text{max}}-1} \int_{z(a)+kp}^{z(a)+(k+1)p} dz f[x(z), \lambda z] \frac{dx(z)}{dz} + \int_{z(a)+k_{\text{max}}p}^{z(b)} dz f[x(z), \lambda z] \frac{dx(z)}{dz}, \quad k_{\text{max}}p < z(b) - z(a).$$

The second integral is of the order of  $p \ll 1$  and can be neglected. In the first term, we shift the integration variable as  $z \rightarrow z + kp$  and use the periodicity of  $f(x, y)$  with respect to the second variable. Then, due to smoothness of the functions  $f(x, y)$  and  $z(x)$  with respect to  $x$ , we approximately replace the summation over  $k$  to the integration over  $z$  and then return to the integration over  $x$  within the initial interval  $(a, b)$ , whereas the integral over the second variable reduces to ‘‘averaging over the phase’’  $u = \lambda z$ ,

$$A(\lambda) \approx \int_a^b dx \int_0^{2\pi} \frac{du}{2\pi} f(x, u). \quad (21)$$

Within such approximation, the first term in Eq. (17) is

$$2D \int_0^{\Delta} dE \int_0^{2\pi} \frac{du}{2\pi} \frac{1}{D^2 + 4R \sin^2[\gamma(E) - u]} = \frac{2\Delta}{1+R}, \quad (22)$$

whereas the second one is

$$\int_{\Delta}^{\infty} dE \int_0^{2\pi} \frac{du}{2\pi} \left\{ \frac{2E[2\xi + D(E - \xi)]}{[2\xi + D(E - \xi)]^2 + 4R\Delta^2 \sin^2 u} - \frac{E}{\xi} \right\} = -\Delta \frac{1+R}{2R} \left( 1 - \frac{D}{\sqrt{R}} \arctan \sqrt{R} \right), \quad (23)$$

which yields the final expression for the excess current,

$$I^{\text{exc}} = \frac{\Delta}{eR_N} \frac{D}{R} \left( \frac{1+R}{\sqrt{R}} \arctan \sqrt{R} - \frac{D}{1+R} \right), \quad L \gg \xi_N. \quad (24)$$

In the limits  $D \ll 1$  and  $R \ll 1$ , Eq. (24) reads

$$I^{\text{exc}} = \frac{\Delta}{eR_N} \begin{cases} \pi D/2, & D \ll 1, \\ 8/3, & R \ll 1. \end{cases} \quad (25)$$

By contrast to the case  $L \ll \xi_N$ , where both contributions to the excess current are small ( $\sim D$ ) at small transparencies  $D$ , the main terms in Eqs. (22) and (23) are of the order of unity. However, they have opposite signs and almost compensate each other, which results in small value ( $\sim D^2$ ) of the excess current in both limits. We note also that the expressions for  $I^{\text{exc}}$  coincide for the short and long junctions in the limit of high transparency,  $R \ll 1$ .

### B. Resonant approximation: IVC at $eV > \Delta$

As we have seen before, the case of the short multichannel junction,  $L < \xi_N$ , can be reduced, within the main approximation over  $L/\xi_N$ , to the case of a short single-channel junction, under appropriate definition of the normal resistance  $R_N$ . A more interesting case, which allows us to obtain simplified results for arbitrary voltages, is the limit of long junction,  $L \gg \xi_N$ . In this case, many Andreev levels are involved in the current transport, their positions are highly sensitive to the propagation angle, and we can apply ‘‘phase averaging’’ method described above for the integration over the energy and angles.

Moreover, in the limit of small transparency, we obtain relatively simple analytical results, by making use the existence of the resonant MAR trajectories, which cross the energy gap through the chain of Andreev levels, when the distance between the levels  $\delta(\mu)$  becomes equal to  $eV$ . This resonant process highly increases the magnitudes of multiparticle currents and makes the IVC non-exponential, at least, at moderately small transparencies; at very small  $D$ , the non-equidistance of the Andreev levels plays role, and the entirely resonant trajectories do not exist (for a more detailed analysis, see Ref. 14).

The single-particle current represents an exclusion: it does not involve Andreev levels and therefore always has a non-resonant nature. At  $D \ll 1$  we have

$$I_1 = \frac{2}{eR_N} \Theta(eV - 2\Delta) \int_0^1 d\mu q(\mu) \int_{-eV/2}^{-\Delta} dE N N_1, \quad (26)$$

where the function

$$N(E, \phi) = \frac{E \xi}{\xi^2 + \Delta^2 \sin^2 \phi(E)} \quad (27)$$

has the meaning of local density of states (DOS). At  $L \gg \xi_N$ , the integrations over  $E$  and  $\mu$  reduces to the averaging of the integrand over two independent phases  $\phi_0$  and  $\phi_1$ , which gives for  $I_1(V)$  a straight Ohmic line starting from the threshold point  $eV = 2\Delta$ ,

$$I_1 = \frac{eV - 2\Delta}{eR_N} \Theta(eV - 2\Delta). \quad (28)$$

The multiparticle currents involve resonant MAR trajectories jumping over consecutive Andreev levels. A general formula for the  $n$ th current ( $n > 1$ ) following from Eq. (11) reads:

$$I_n = \frac{nD^{n-1}}{eR_N} \Theta(neV - 2\Delta) \int_{-neV/2}^{E_{\text{max}}} dE \left\langle \frac{8NN_n}{|Z|^2} \right\rangle, \quad (29)$$

$$E_{\text{max}} = \min[-\Delta, \Delta - (n-1)eV], \quad \frac{2\Delta}{n} \leq eV \leq \frac{2\Delta}{n-2},$$

where the angle brackets denote averaging over two phases mentioned above. In order to take into account only entirely resonant trajectories, we must demand that the energies  $E_k$  of all intermediate Andreev reflections ( $1 \leq k \leq n-1$ ) were located inside the gap, where the Andreev levels exist. This results in the restriction  $E < E_{\text{max}}$  for the initial energy  $E$  in Eq. (29), and in a limited voltage range where given partial current is nonzero within our approximation.

The 2-particle current is a special one and differs from the high order currents: it involves only one intermediate Andreev reflection, and therefore only the initial energy  $E$  should be adjusted in order to achieve the resonant transmission, when  $E_1 = E + eV$  coincides with the Andreev level; the interlevel distance is irrelevant in this aspect. Formally, this manifests itself in appearance of only one resonant phase in the denominator; a characteristic scale for this phase is  $D$ . The second independent phase is non-resonant and varies within the whole interval of periodicity,

$$I_2 = \frac{4}{eR_N} \Theta(eV - \Delta) \int_0^{2\pi} \frac{du}{2\pi} \int_0^{\min(\Delta, eV - \Delta)} \frac{dE}{N_+^{-1} + N_-^{-1}},$$

$$N_{\pm} = N(E \pm eV, \phi_{\pm}), \quad \phi_{\pm} = \gamma(E) \pm u. \quad (30)$$

For symmetry, we actually used  $E_1$  as the integration variable  $E$  in Eq. (30). We note that due to resonant transmission through the intermediate Andreev level, the 2-particle current appears to be of similar order  $D$  as the single-particle one. This result was already discovered during the calculation of the excess current; the latter, however, was found to be of the order of  $D^2$  due to cancelation of main terms in the 2-particle current and in the ‘‘deficit’’ part of the 1-particle current.

### C. IVC at $eV < \Delta$

We will present here a semi-quantitative description of the IVC at smaller applied voltage,  $eV < \Delta$ , when the partial currents with the numbers  $n > 2$  are relevant. It follows from the analysis for the single-mode contact,<sup>14</sup> that the IVC exhibits a complex pattern of current peaks resulting from the multiple Andreev resonances. Integration over the angle will smoothen this pattern; however, one should expect that the reduced oscillations will remain since the 2D density of Andreev levels has the peaks due to enhanced contribution of the reference point  $\theta = 0$  ( $\mu = 1$ ).

To develop qualitative understanding of the behavior of IVC, we consider long junctions with small Andreev level spacing,  $\delta(E) \ll \Delta$ . We anticipate that the resonant processes will mostly contribute to the current, therefore we will consider only these contributions, and evaluate them within the model of equidistant Andreev spectrum,  $\delta(E) = \text{const}$ . This model can be only justified because of its good agreement with the numerical simulations. The agreement can be explained with the numerical fact that for all the transparencies (except of the very small ones) the energy width of the multiparticle resonances,  $\sim \delta\sqrt{D}$ , is not much smaller than the non-equidistance of the Andreev levels.

In the resonance approximation, the main contribution to the  $n$ -particle current comes from the resonant MAR paths.

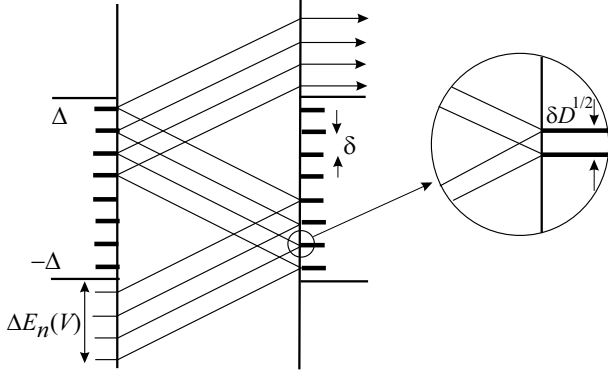


FIG. 8. Resonant MAR trajectories passing through the Andreev levels (short bold lines) and contributing to the 3-particle current at  $L = 10\xi_N$  and  $eV = 4\delta$ . The inset shows splitting of a static Andreev level to the cluster consisting of 2 levels, therefore the whole number of the resonant trajectories is 8 in this case.

These paths are those when all  $n-1$  Andreev reflections occur at the resonance energies within the superconducting gap, i.e., the voltage is commensurate with the level spacing,  $eV = k\delta$ , and it is smaller than  $V < V_{n-2}$ , i.e., belongs to the interval  $V_n < V < V_{n-2}$  ( $V_n = 2\Delta/n$ ). Such trajectories, shown in Fig. 8 for the 3-particle current, give the contribution to the current spectral density  $j_n \sim D(E, E + neV)$ , where the quantity

$$D(E_m, E_n) = |(\hat{M}_{mn})_{11}|^{-2} \quad (31)$$

has the meaning of the effective transparency of MAR chains between the points  $E_n$  and  $E_m > E_n$  at the energy axis. Such a resonant MAR process is mapped onto a periodic  $n$ -barrier tunnel structure with resonant levels in each well having the same energy when the barriers are non-transparent.<sup>18</sup> At the finite barrier transparency, the levels will repel each other forming a tight cluster of resonant levels within the energy interval  $\sim \delta\sqrt{D}$  (precursor of the energy band at  $n \rightarrow \infty$ ), as shown in the inset in Fig. 8. This leads to the splitting of the resonant transmissivity of the whole structure into  $n-1$  peaks at the energy axis and results in the following schematic structure of the function

$$D(E, E_n) = \frac{D^n}{\prod_{k=1}^{n-1} (\varepsilon/\delta - a_k\sqrt{D})^2 + \Lambda^2} \quad (32)$$

for a single conducting channel.<sup>14</sup> Here  $a_k$  are numerical constants describing distribution of the resonant levels over the cluster, and  $\varepsilon$  is the deviation of the MAR chain from the resonant position in the energy space. The maximum value and the width of the resonance in Eq. (32) is determined by the magnitude of the second term in the denominator, which is of the order of  $n^2D^n$  for large  $n$ ; a better approximation to the numerical result at  $n > 2$  is given by the estimate  $\Lambda^2 \approx (n-1)^2D^n$ . This results in the peak height  $\sim 1/(n-1)^2$  and the width  $(n-1)D\delta$ , the latter being much smaller than the distance  $\delta\sqrt{D}$  between the levels within the cluster.

All peaks within the resonant region  $\delta\sqrt{D}$  give independent

contributions into the total current,

$$J_n[\text{path}] \sim \frac{2e}{h} n \sum_{j=1}^{n-1} \int_{-\infty}^{\infty} d\varepsilon \frac{D^2 \delta^2}{\varepsilon^2 + [(n-1)a_j D \delta]^2} \sim \frac{2e}{h} n D \delta. \quad (33)$$

This is contribution to the current from a single resonant cluster. The number of such contributions can be estimated as  $\Delta E_n(V)/\delta$ , where  $\Delta E_n(V)$  is the width of the interval of the energy integration, in which the resonant MAR trajectories exist (see Fig. 8, where four resonant sets of MAR trajectories are depicted). If the voltage  $V < V_{n-1}$ , then this interval is  $\Delta E_n(V) = neV - 2\Delta = 2\Delta(V/V_n - 1)$  and increases with voltage; at larger voltage,  $V > V_{n-1}$ , the quantity  $\Delta E_n(V) = 2\Delta(1 - V/V_{n-2})$  decreases and turns to zero at  $V = V_{n-2}$ .

Thus, the resonant magnitude of the  $n$ -th current at  $eV = k\delta$  is given by

$$J_n^{\text{res}} \sim \frac{2e}{h} n D \Delta E_n(V) \quad (34)$$

and approaches maximum value  $(2e/h)2n\Delta D/(n-1)$  at  $V = V_{n-1}$ . The width of the resonance in voltage can be estimated as follows. The deviation in voltage,  $\Delta(eV)$ , from its resonant value  $eV = k\delta$  results in deviation of the distance  $(n-2)\Delta(eV)$  between the first and the last  $n-1$  subgap Andreev reflections. In order to hold the resonant transmissivity, the latter value should not exceed the width of the resonant region  $\delta\sqrt{D}$ . As the result, the width of the voltage peak at the single-channel IVC<sup>14</sup> is

$$\Delta(eV) \sim \delta\sqrt{D}/(n-2). \quad (35)$$

In a multichannel junction, the resonant current magnitude in Eq. (34) can be achieved at arbitrary subgap voltage by tuning the level spacing  $\delta(\mu) = \mu\delta_m$  [a more precise estimate is given by Eq. (13)]. Thus, the main contribution to  $J_n$  comes from narrow vicinities of the resonant level spacings,  $\delta_k = \mu_k\delta_m = eV/k$ . The width  $\Delta(\mu)$  of the resonant regions of  $\mu$  can be estimated similar to the width of the voltage peak in a single-channel case: the deviation in  $\delta$ ,  $\Delta(\delta) = \Delta(\mu)\delta_m$ , times the number of levels  $eV(n-2)/\delta$  between the first and the last subgap Andreev reflections, should not exceed  $\delta\sqrt{D}$ ,

$$\Delta(\mu) \sim \frac{\delta^2\sqrt{D}}{eV(n-2)\delta_m} \quad (36)$$

and therefore the contribution from a given resonant value  $\delta_k$  to the current is

$$\begin{aligned} J_n^{(k)} &\sim \mathcal{N} j_n^{\text{res}} [\Delta(\mu)q(\mu)]_{\mu=\mu_k} \quad (37) \\ &= C \frac{2e}{h} \mathcal{N} \frac{nD^{3/2}\Delta E_n(V)}{eV(n-2)\delta_m} \left(\frac{eV}{k}\right)^2 q\left(\frac{eV}{k\delta_m}\right). \end{aligned}$$

Since  $\delta_k$  can not exceed  $\delta_{\text{max}}$ , the contributions to the net current  $I_n$  come from  $I_n^{(k)}$  with the numbers  $k_{\text{min}} = \text{Int}(eV/\delta_m) + 1 \leq k < \infty$ . Thus, expressing the number of channels  $\mathcal{N}$  through the normal resistance, we obtain final expression for the  $n$ -particle current,

$$I_n = C \frac{n\Delta E_n(V)\sqrt{D}}{eR_N(n-2)\delta_m} \sum_{k=k_{\text{min}}}^{\infty} \frac{eV}{k^2} q\left(\frac{eV}{k\delta_m}\right), \quad n > 2, \quad (38)$$

where  $C$  is a numerical constant. The value of this constant,  $C = 0.6$ , is found by comparing Eq. (38) with the result of exact calculation of multiparticle currents by using Eq. (32) in the equidistant spectrum approximation (see Appendix).

At  $eV \gg \delta_m$  ( $k_{min} \gg 1$ ), we can approximately replace the summation over  $k$  by integration and obtain for both the 2D and 3D cases

$$I_n(V) = C \frac{n\Delta E_n(V)\sqrt{D}}{eR_N(n-2)}. \quad (39)$$

In such approximation, the partial currents with numbers  $n > 2$ , as functions of voltage, have the shape of triangles with the bases between  $V_n$  and  $V_{n-2}$  and with the apex at  $V_{n-1}$  having the amplitude  $2n\Delta\sqrt{D}/eR_N(n-1)(n-2)$ . The net current  $I(V)$  at given voltage  $V$  ( $V_n < V < V_{n-1}$ ) contains contributions from two consequent partial currents  $I_n$  (increasing arm) and  $I_{n+1}$  (decreasing arm), and therefore the IVC represents piece-wise linear function connecting apexes of the triangles,

$$I(V) = \frac{C\sqrt{D}}{R_N(n-2)} \left[ (n+2)V - \frac{4\Delta}{e(n-1)} \right], \quad (40)$$

$$V_n < V < V_{n-1}, \quad n > 2.$$

Its behavior at the edges of of the subgap region is described by following expressions,

$$I(V) = C \frac{\sqrt{D}}{R_N} \begin{cases} 5V - 2\Delta/e, & eV > 2\Delta/3, \\ V(1 + eV/\Delta), & \delta_m \ll eV \ll \Delta. \end{cases} \quad (41)$$

At smaller voltages,  $eV < \delta_m$ , Eq. (38) describes power-like decay of current with voltage,  $I(V) \sim V^3$ .

Equations (40) and (41), as well as the more general Eq. (38), clearly demonstrate the universality of the averaged IVC found by the numerical computation: The smooth part of the dc current at  $eV < \Delta$  is the universal function of the applied voltage, it is independent of the junction length, and scales as the 3/2 power of the junction transparency.

The comparison between the results of numerical calculation and analytical approach is shown in Fig. 9 where both the general Eq. (38) (blue solid line) and its averaged form Eq. (40) (dashed line) were plotted. We see that Eq. (38) also describes oscillations of the IVC revealed in numerical computation with sharp peaks at the resonant voltages  $eV = k\delta_m$  related to the electron trajectories at the reference point  $\mu = 1$ . In the 2D case, due to divergence of the geometric weight  $q(\mu)$  at the reference point, the formal calculation of IVC by means of Eq. (38) leads to singularities of  $I(V)$  at the resonant voltages. A simple regularization of the geometric weight  $q(\mu)$  by a small shift of the singularity to the region  $\mu > 1$  eliminates these divergencies. The figure shows satisfactory agreement between the numerical and analytical results, except the absence of the excess current in the approximate expressions, Eqs. (28) and (30), for the 1- and 2-particle currents. Similar conclusion is valid for the 3D junction; in this case, no additional regularization is needed since the geometric weight is non-singular.

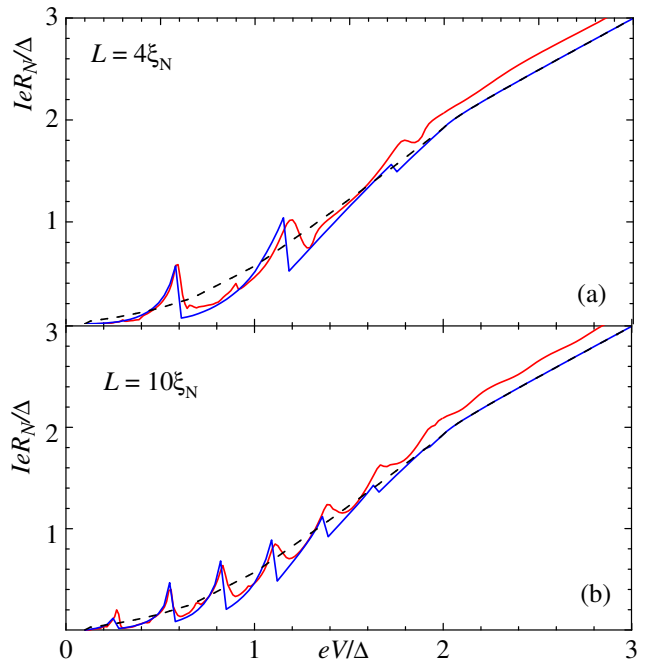


FIG. 9. (Color online) Analytically calculated IVC [Eq. (38), blue solid line] and its averaged form [Eqs. (28), (30) and (40), dashed curve], in comparison with the result of numerical computation (red solid curve) for a 2D junction with the transparency  $D = 0.1$  and length  $L = 4\xi_N$  (a), and  $L = 10\xi_N$  (b).

## V. SUMMARY

In this paper we investigate, both numerically and analytically, the dc current transport at given applied voltage through the ballistic SNINS junction of finite length  $L$  and width. In particular, such model corresponds to the experimental setup with the normal 2D electron gas confined by massive superconducting electrodes and controlled by a narrow electrostatic gate playing the role of a tunable tunnel barrier of moderately low transparency  $D$  (Josephson field-effect transistor). Using the coherent multiple Andreev reflections formalism, we found that the characteristic features of the charge transfer in this device are fully determined by the presence of bound Andreev states. These states produce singularities in the quasiparticle density of states and therefore provide conditions for the resonant transmissivity.

In the limit of a short junction,  $L < \xi_N$ , when only one pair of the levels exist for most of quasiparticles (except those propagating at small angles to the interfaces), the IVC resembles the one of a single channel point contact, namely, the current decays exponentially with the voltage and exhibits a typical subharmonic structure periodic in  $1/V$ . However, in junctions with small but finite length, the role of the energy parameter that defines the period of subharmonics and also the decrement of the exponential current decay is played by the Andreev interlevel distance  $\delta_m$  rather than the superconducting energy gap in the case of the point contact.

The most interesting phenomena were predicted for long junctions with multiple Andreev levels. Existence of fully resonant MAR trajectories passing through the chain of the levels

essentially enhances the subgap current at voltages commensurate with the level spacing thus creating a resonance periodic structure in  $V$  with the period  $\delta_n/e$ . Furthermore, the averaged IVC has a power form, and exhibits a peculiar universality: it does not depend on the junction length, and is universal for all junction transparencies at  $eV < \Delta$  being normalized by  $\sqrt{D}/R_N$ . Physical explanation of these characteristic features, discovered in numerics, are given within the framework of theory of resonant MAR charge transfer.

Finally, we note that both resonant effects - subharmonics of the interlevel distance in short junctions and its harmonics in long ones - can be used for direct experimental probing of Andreev levels in ballistic SNS structures.

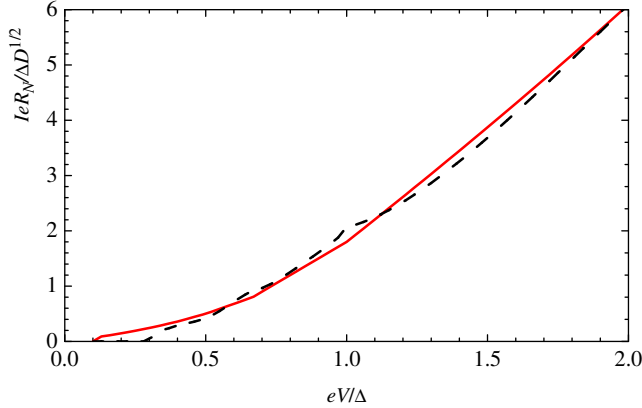


FIG. 10. Subgap IVC calculated from Eq. (40) with the fitting constant  $C = 0.6$  (solid line), compared with the sum of seven partial currents evaluated from Eqs. (A.1)–(A.3) (dashed line).

### Appendix: Multiparticle currents

In this Section we present analytical expressions for several multiparticle currents  $I^{(n)}$  calculated in the limits  $D \ll 1$ ,

$L \gg \xi_N$  by making use of explicit expression of the quantity  $D(E, E_n)$  taken in the approximation of equidistant Andreev levels. While  $n$  increases, the complexity of expressions for  $I^{(n)}$  tremendously enhances; for this reason we restrict our examples by the currents with  $n = 3 \div 5$ ,

$$I^{(3)} = \frac{3\sqrt{D}}{eR_N} \int_{-3eV/2}^{E_{\max}} dE \sqrt{N_0 N_3}, \quad (\text{A.1})$$

$$E_{\max} = \min(-\Delta, \Delta - 2eV), \quad 2/3 < eV/\Delta < 2,$$

$$\phi_0 = 2\gamma_1 - \gamma_2, \quad \phi_3 = 2\gamma_2 - \gamma_1.$$

$$I^{(4)} = \frac{2\sqrt{D}}{eR_N} \int_{-2eV}^{E_{\max}} \frac{N_0 N_4 dE}{N_0 + N_4} \left[ \left( \frac{N_0}{N_4} \right)^{1/4} + \left( \frac{N_4}{N_0} \right)^{1/4} \right], \quad (\text{A.2})$$

$$E_{\max} = \min(-\Delta, \Delta - 3eV), \quad 1/2 < eV/\Delta < 1,$$

$$\phi_0 = (1/2)(3\gamma_1 - \gamma_3), \quad \phi_4 = (1/2)(3\gamma_3 - \gamma_1).$$

$$I^{(5)} = \frac{20\sqrt{2D}}{\pi eR_N} \int_{-5eV/2}^{E_{\max}} dE \left[ \int_0^{y_-} + \int_{y_+}^{\infty} \right] dy \times \frac{N_0 N_5 N_+ (y-2) \sqrt{y/R(y)}}{(y-2)^2 [R(y) + 8y^2] N_{\pm}^2 - R(y)(3y-2)^2 N_{\pm}^2} \quad (\text{A.3})$$

$$R(y) = y^2 - 3y + 1, \quad y_{\pm} = (1/2)(3 \pm \sqrt{5}), \quad N_{\pm} = N_0 \pm N_5,$$

$$E_{\max} = \min(-\Delta, \Delta - 4eV), \quad 2/5 < eV/\Delta < 2/3,$$

$$\phi_0 = 3\gamma_2 - 2\gamma_3, \quad \phi_5 = 3\gamma_3 - 2\gamma_2.$$

Here  $N_n = N(E + neV, \phi_n)$  is the density of states defined in Eq. (27), and  $\gamma_k = \arccos[(E + keV)/\Delta]$ .

Such method allows us to describe only the smooth part of the IVC and gives the shape of  $I(V)$  result very close to Eq. (40) that allows us to determine the fitting constant  $C = 0.6$  in Eq. (40) and, correspondingly, in Eq. (38). The result of such fitting is shown in Fig. 10, where the dashed line is the sum of seven partial currents obtained in an analytically tractable form.

- 
- <sup>1</sup> H. Takayanagi and T. Kawakami, Phys. Rev. Lett. **54**, 2449 (1985).
  - <sup>2</sup> H. Takayanagi, T. Akazaki, and J. Nitta, Phys. Rev. Lett. **75**, 3533 (1995).
  - <sup>3</sup> T. Schäpers, Superconductor/Semiconductor Junctions (Springer, Berlin, 2001).
  - <sup>4</sup> A. Chrestin, R. Kürsten, K. Biedermann, T. Matsuyama, and U. Merkt, Superlattices Microstruct. **25**, 711 (1999).
  - <sup>5</sup> T. Akazaki, H. Takayanagi, J. Nitta, and T. Enoki, Appl. Phys. Lett. **68**, 418 (1996).
  - <sup>6</sup> P. Samuelsson, Å. Ingerman, G. Johansson, E. V. Bezuglyi, V. S. Shumeiko, G. Wendin, R. Kürsten, A. Richter, T. Matsuyama, and U. Merkt, Phys. Rev. B **70**, 212505 (2004).
  - <sup>7</sup> T. D. Clark, R. J. Prance, and A. D. C. Grassie, J. Appl. Phys **51**, 2736 (1980).
  - <sup>8</sup> A. D. Zaikin and G. F. Zharkov, Zh. Eksp. Teor. Fiz. **78**, 721 (1978) [Sov. Phys. JETP **51**, 364 (1980)].
  - <sup>9</sup> A. D. Zaikin and G. F. Zharkov, Zh. Eksp. Teor. Fiz. **81**, 1781 (1981) [Sov. Phys. JETP **54**, 944 (1981)];
  - <sup>10</sup> A. D. Zaikin and G. F. Zharkov, Pis'ma Zh. Eksp. Teor. Fiz. **35**, 465 (1982) [JETP Lett. **35**, 636 (1982)].
  - <sup>11</sup> E.N. Bratus', V.S. Shumeiko, and G. Wendin, Phys. Rev. Lett. **74**, 2110 (1995).
  - <sup>12</sup> D. Averin and A. Bardas, Phys. Rev. Lett. **75**, 1831 (1995).
  - <sup>13</sup> J. C. Cuevas, A. Martín-Rodero, and A. Levy Yeyati, Phys. Rev. B **54** 7366 (1996).
  - <sup>14</sup> Å. Ingerman, G. Johansson, V. S. Shumeiko, and G. Wendin, Phys. Rev. B **64**, 144504 (2001).
  - <sup>15</sup> E. V. Bezuglyi, A. S. Vasenko, E. N. Bratus', V. S. Shumeiko, and G. Wendin, Phys. Rev. B **73**, 220506(R) (2006).
  - <sup>16</sup> E. V. Bezuglyi, E. N. Bratus', and V. S. Shumeiko, Phys. Rev. B **83**, 184517 (2011).
  - <sup>17</sup> A. V. Zaitsev and D. V. Averin, Phys. Rev. Lett. **80**, 3602 (1998).
  - <sup>18</sup> G. Johansson, G. Wendin, K. N. Bratus, V. S. Shumeiko, Superlatt. Microstruct. **25**, 905 (1999).
  - <sup>19</sup> G. de Gennes and D. Saint-James, Phys. Lett. **4**, 151 (1963).
  - <sup>20</sup> B. A. Aminov, A. A. Golubov, and M. Yu. Kupriyanov, Phys. Rev. B **53**, 365 (1996).
  - <sup>21</sup> E. V. Bezuglyi, E. N. Bratus', and V. S. Shumeiko, Physica C **499**, 15 (2014).